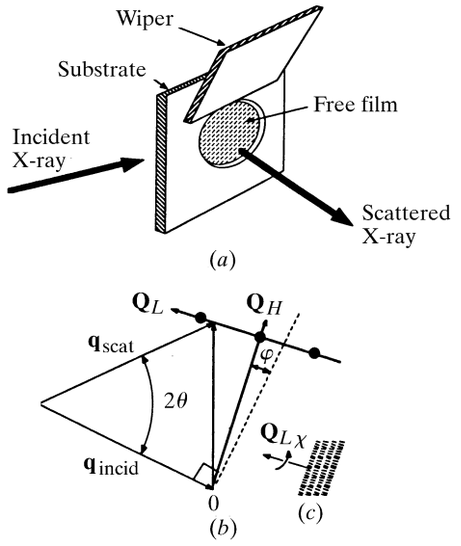

Fig. 4.4.4.1. (*a*) Schematic illustration of the geometry and (*b*) kinematics of X-ray scattering from a freely suspended smectic film. The insert (*c*) illustrates the orientation of the film in real space corresponding to the reciprocal-space kinematics in (*b*). If the angle $\varphi = \theta$, the film is oriented such that the scattering vector is parallel to the surface of the film, *i.e.* parallel to the smectic layers. A 'Q_L scan' is taken by simultaneous adjustment of φ and 2θ to keep $(4\pi/\lambda)\sin(\theta)\cos(\theta - \varphi) = (4\pi/\lambda)\sin(\theta_{100})$, where θ_{100} is the Bragg angle for the 100 reflection. The different in-plane Bragg reflections can be brought into the scattering plane by rotation of the film by the angle χ around the film normal.

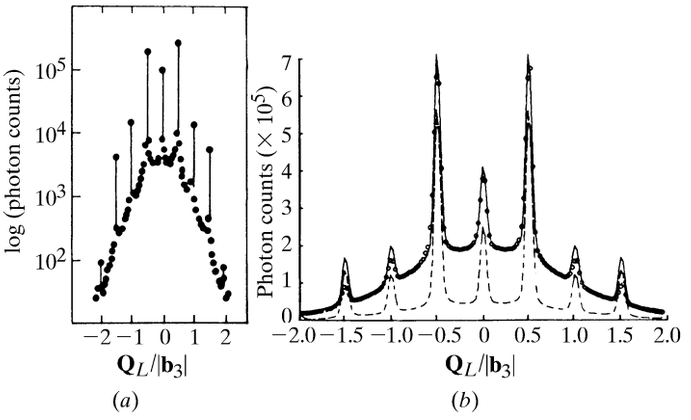

Fig. 4.4.4.2. Typical Q_L scans from the crystalline-B phases of (*a*) a free film of 7O.7, displayed on a logarithmic scale to illustrate the reduced level of the diffuse scattering relative to the Bragg reflection and (*b*) a bulk sample of 4O.8 oriented by a magnetic field.

reflected intensities for films of 2, 3, 4, 5, . . . layers are in the ratio of 4, 9, 16, 25, . . ., the measurement can be calibrated by drawing and measuring a reasonable number of thin films. The most straightforward method for thick films is to measure the ellipticity of the polarization induced in laser light transmitted through the film at an oblique angle (Collett, 1983; Collett *et al.*, 1985); however, a subtler method that makes use of the colours of white light reflected from the films is also practical (Sirota, Pershan, Sorensen & Collett, 1987). In certain circumstances, the thickness can also be measured using the X-ray scattering intensity in combination with one of the other methods.

Fig. 4.4.4.1 illustrates the scattering geometry used with these films. Although recent unpublished work has demonstrated the possibility of a reflection geometry (Sorensen, 1987), all of the X-ray scattering studies to be described here were performed in transmission. Since the in-plane molecular spacings are typically between 4 and 5 Å, while the layer spacing is closer to 30 Å, it is difficult to study the 00*L* peaks in this geometry.

Fig. 4.4.4.2 illustrates the difference between X-ray scattering spectra taken on a bulk crystalline-B sample of *N*-[4-(*n*-butyloxy)-benzylidene]-4-*n*-octylaniline (4O.8) that was oriented in an external magnetic field while in the nematic phase and then cooled through the smectic-A phase into the crystalline-B phase (Aeppli *et al.*, 1981), and one taken on a thick freely suspended film of *N*-[4-(*n*-heptyloxy)benzylidene]-4-*n*-heptylaniline (7O.7) (Collett *et al.*, 1982, 1985). Note that the data for 7O.7 are plotted on a semi-logarithmic scale in order to display simultaneously both the Bragg peak and the thermal diffuse background. The scans are along the $\mathbf{Q}_L$ direction, at the appropriate value of $\mathbf{Q}_H$ to intersect the peaks associated with the intralayer periodicity. In both cases, the widths of the Bragg peaks are essentially determined by the sample mosaicity and as a result of the better alignment the ratio of the thermal diffuse background to the Bragg peak is nearly an order of magnitude smaller for the free film sample.

4.4.4.1. *Hexatic phases in two dimensions*

The hexatic phase of matter was first proposed independently by Halperin & Nelson (Halperin & Nelson 1978; Nelson & Halperin 1979) and Young (Young, 1979) on the basis of theoretical studies of the melting process in two dimensions. Following work by Kosterlitz & Thouless (1973), they observed that since the interaction energy between pairs of dislocations in two dimensions decreases logarithmically with their separation, the enthalpy and the entropy terms in the free energy have the same functional dependence on the density of dislocations. It follows that the free-energy difference between the crystalline and hexatic phase has the form $\Delta F = \Delta H - T\Delta \boldsymbol{S} \approx T_c \boldsymbol{S}(\rho) - T\boldsymbol{S}(\rho) = \boldsymbol{S}(\rho)(T_c - T)$, where $\boldsymbol{S}(\rho) \approx \rho \log(\rho)$ is the entropy as a function of the density of dislocations ρ and T_c is defined such that $T_c\boldsymbol{S}(\rho)$ is the enthalpy. Since the prefactor of the enthalpy term is independent of temperature while that of the entropy term is linear, there will be a critical temperature, T_c, at which the sign of the free energy changes from positive to negative. For temperatures greater than T_c, the entropy term will dominate and the system will be unstable against the spontaneous generation of dislocations. When this happens, the two-dimensional crystal, with positional QLRO, but true long-range order in the orientation of neighbouring atoms, can melt into a new phase in which the positional order is short range, but for which there is QLRO in the orientation of the six neighbours surrounding any atom. The reciprocal-space structures for the two-dimensional crystal and hexatic phases are illustrated in Figs. 4.4.4.3(*b*) and (*c*), respectively. That of the two-dimensional solid consists of a hexagonal lattice of sharp rods (*i.e.* algebraic line shapes in the plane of the crystal). For a finite size sample, the reciprocal-space structure of the two-dimensional hexatic phase is a hexagonal lattice of diffuse rods and there are theoretical predictions for the temperature dependence of the in-plane line shapes (Aeppli & Bruinsma, 1984). If the sample were of infinite size, the QLRO of the orientation would spread the six spots continuously around a circular ring, and the pattern would be indistinguishable from that of a well correlated liquid, *i.e.* Fig. 4.4.4.3(*a*). The extent of the patterns along the rod corresponds to the molecular form factor. Figs. 4.4.4.3(*a*), (*b*) and (*c*) are drawn on the assumption that the molecules are normal to the two-

references